ARTICLE NO. 80-4090

J80-210

10015
20003
20011

Study of the Insulating Wall Boundary Layer in a Faraday MHD Generator

Roy R. Rankin,* Sidney A. Self,† and Robert H. Eustis‡
High Temperature Gasdynamics Laboratory, Stanford University, Stanford, Calif.

An experimental and analytical investigation of the insulating wall boundary layer in an operating MHD generator was undertaken. Velocity profiles were measured by a laser anemometer technique and the results compared with the finite difference solution of the momentum, energy, and electrical equations accounting for variable equilibrium properties. Both experimental and theoretical results showed a velocity overshoot near the wall for subsonic flow with an attendant increase in friction factor and Stanton number over that expected without MHD effects. The calculations were extended to larger size MHD generators; and for a subsonic pilot plant unit, an increase of the sidewall friction factor of over 150% was indicated with a 50% increase in Stanton number. Calculations for a supersonic generator showed that flow separation may occur on the sidewall because of the current pattern caused by the temperature overshoot common in supersonic boundary layers.

Nomenclature

A	= area
A^+	= Van Driest constant
B	= magnetic field strength
D	= damping function
d	= diameter
$\bar{E}, E_x, E_y$	= electric field vector and components
F	= frequency
f	= focal length
H	= total enthalpy
$\bar{J}, J_x, J_y$	= current density vector and components
K	= load parameter
ℓ	= mixing length
P	= static pressure
Pr	= Prandtl number
$\dot{q}_{rad}$	= total radiation from gas per unit volume
T	= static temperature
u	= velocity in x direction
w	= velocity in z direction
x,z	= spatial coordinates (Fig. 1)
z^+	= distance from insulating wall in "wall coordinates"
β	= Hall parameter
δ_{99}	= 99% boundary layer thickness
κ	= mixing length constant
λ	= mixing length cut-off parameter or wavelength of light
ρ	= density
σ	= electrical conductivity or Stefan-Boltzmann constant
τ	= shear stress
μ, μ_t, μ_{eff}	= molecular, turbulent, and effective viscosity

I. Introduction

IN contrast to conventional duct flow, for MHD generators the boundary layers on adjacent walls experience different body forces and joule heating with associated variations in friction and heat transfer. This is because of the electric current which must pass through the electrode boundary layer where it is generally considered uniform (except near the corners) but which may vary greatly through the insulator wall boundary layer according to the conductivity and velocity profiles. Electrode voltage drops have been a major interest in MHD generator development and consequently the electrode boundary layer has been studied by several investigators.[1,2] The pioneering work of Hartmann and Lazarus[3] showed that the insulator wall velocity profile in a liquid metal flow could be modified by electromagnetic effects with a concomitant effect on wall friction. Other investigators extended this work[4] and Sonju[5] showed the significance of the Hartmann phenomenon in a combustion-driven MHD channel with no net current flow.

The electromagnetic effects on the insulator wall boundary layer were not considered in early efforts to correlate measured MHD generator pressure distributions with predictions. Louis et al.[6] found that the calculated pressure distribution agreed well with the measured distribution. On the other hand, Teno et al.[7] found that to get reasonable agreement the skin friction coefficient had to be increased by a factor of three from the fully rough value to obtain good agreement with the data. Similarly, Sonju et al.[8] found good agreement at low generator output levels, but poor agreement at higher output levels. The motivation of the present work was to understand these apparent discrepancies, and it is suggested that the presence of extended Hartmann flow can in part explain the observations.

In constant property MHD flows the current density varies across the insulating wall boundary layer due to a decrease in velocity toward the wall. The current interacts with the external magnetic field to produce a varying body force across the boundary layer which modifies the velocity profile from that existing in the absence of MHD interaction. This phenomenon is known as Hartmann flow. In a gaseous plasma the variation of temperature and, hence, electrical conductivity, across the boundary layer has a further effect on the current density. The inclusion of variable properties thus can result in additional alteration of the current and of the fluid flow. Hartmann flow with the inclusion of variable properties has been called, in this work, "extended Hartmann flow" and is the primary concern of this study.

The investigation reported here includes a numerical solution of the insulating wall boundary layer equations which include electromagnetic effects in their formulation. Predictions are made of both the temperature and velocity

Received Oct. 3, 1979; revision received Jan. 29, 1980. Copyright © American Institute of Aeronautics and Astronautics, Inc., 1980. All rights reserved.

Index categories: Plasma Dynamics and MHD; MHD; Boundary Layers and Convective Heat Transfer—Turbulent.

*Currently Postdoctoral Fellow at the University of Sydney, Australia.

†Adjunct Professor of Mechanical Engineering. Member AIAA.

‡Professor of Mechanical Engineering. Associate Fellow AIAA.

profiles and the associated Stanton number and friction coefficient. An experimental determination of the velocity profile in an operating MHD generator was made using a laser anemometer developed in the Stanford High Temperature Gasdynamics Laboratory. Comparison of the numerical and experimental results was satisfactory and showed clearly the major importance of the extended Hartmann effect in influencing the insulator wall boundary layer. Extension of the predictions to a pilot plant size MHD generator shows a two-fold increase in friction factor (compared to a similar prediction not including the extended Hartmann effect) and a 20% increase in the Stanton number.

II. Model and Computational Procedure

A schematic diagram of a segmented Faraday-type MHD generator is shown in Fig. 1. The working fluid of the generator, which in the present work was the products of combustion of ethanol with a small fraction of potassium added to form a partially ionized gas or plasma, flows in the positive x direction. A magnetic field is externally imposed in the positive z direction. The interaction between the flowing ionized gas and the magnetic field generates a current and/or an electric field. In the case of a segmented Faraday generator, the current flows in the negative y direction. This current is transmitted to external loads by electrodes on the top and the bottom of the channel. The insulating walls of the generator are the walls which are normal to the magnetic field. It is the boundary layers on these walls that are the subject of this work.

In the case of classical Hartmann flow, the assumptions of steady, laminar, incompressible, fully-developed channel flow of a conducting fluid with an applied magnetic field normal to the flow axis are made. This flow has been treated in the texts by Sutton and Sherman[9] and Mitchner and Kruger,[10] for example. In a gaseous plasma the variation of temperature, and hence electrical conductivity, across the boundary layer has an important additional effect on the current density as compared to constant property Hartmann flow. In this extended Hartmann flow with variable properties, the energy equation and the momentum equation are coupled so that a numerical solution is required.

The basic equations for extended Hartmann flow consist of the two-dimensional boundary-layer equations including MHD effects, where momentum terms in the y direction and three-dimensional effects have been neglected as being small. The equations for the core of the channel are the special case of the boundary-layer equations without gradient terms. The assumption that three-dimensional effects can be neglected will become more accurate as the aspect ratio of the channel increases. To minimize the corner effects on the present model and measurements, only the center of the insulating wall was investigated. Ohm's law in two dimensions including Hall effect is used. The basic time-averaged equations are as follows:

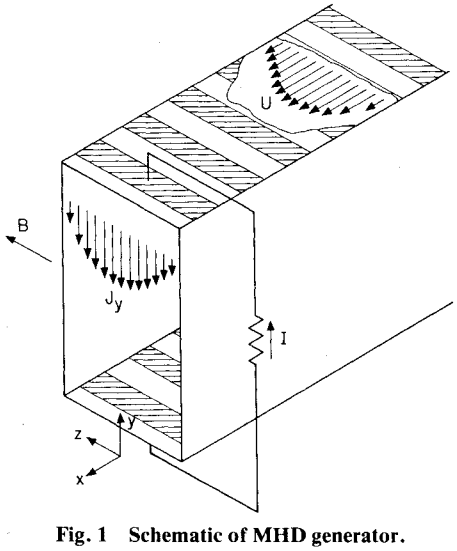

Fig. 1 Schematic of MHD generator.

Continuity

$$\frac{\partial(\rho u)}{\partial x}+\frac{\partial(\rho w)}{\partial z}=0 \tag{1}$$

Momentum

$$\rho u\frac{\partial u}{\partial x}+\rho w\frac{\partial u}{\partial z}=J_yB-\frac{\mathrm{d}P}{\mathrm{d}x}+\frac{\partial}{\partial z}\left(\mu_{\mathrm{eff}}\frac{\partial u}{\partial z}\right) \tag{2}$$

Energy

$$\rho u\frac{\partial H}{\partial x}+\rho w\frac{\partial H}{\partial z}=\frac{1}{Pr}\frac{\partial}{\partial z}\left(\mu_{\mathrm{eff}}\frac{\partial H}{\partial z}\right)+\left(1-\frac{1}{Pr}\right)\frac{\partial}{\partial z}\times\left[\mu_{\mathrm{eff}}\frac{\partial}{\partial z}\left(\frac{u^2}{2}\right)\right]+\boldsymbol{J}\cdot\boldsymbol{E}+\dot{q}_{\mathrm{rad}} \tag{3}$$

Ohm's Law

$$J_x=\frac{\sigma}{1+\beta^2}\left[E_x-\beta(E_y-uB)\right] \tag{4a}$$

$$J_y=\frac{\sigma}{1+\beta^2}\left[E_y-uB+\beta E_x\right] \tag{4b}$$

The boundary conditions at the wall are that the enthalpy is specified and the velocity is zero. At the outer edge of the boundary layer either the enthalpy and velocity are specified or a symmetry condition is invoked as discussed in the section on numerical methods. The basic equations do not represent a closed set of equations. To close the set, equations of state, a turbulence model, and an electrical model are needed.

The equations of state used for the plasma properties were curve fits to thermochemical equilibrium calculations for the products of combustion of alcohol burned in oxygen with nitrogen added and seeded with potassium hydroxide. These curve fits and equilibrium computations are discussed in Refs. 11 and 12.

An eddy viscosity model as described by Kays[13] was used. The expression for the eddy viscosity μ_t is defined through Prandtl's mixing length ℓ as

$$\mu_t=\rho\ell^2\left|\frac{\mathrm{d}u}{\mathrm{d}z}\right| \tag{5}$$

The actual modeling of the mixing length is divided into three different regions. In the near wall region ℓ grows linearly with distance from the wall through the relationship

$$\ell=\kappa z \tag{6}$$

where the proportionality constant κ is usually set to 0.41. In the viscous sublayer, the Van Driest damping function D multiplies Eq. (6) so that $\ell=\kappa zD$. The damping function is

$$D=1.0-\exp(-z^+/A^+) \tag{7}$$

where $z^+=z(\sqrt{\tau\rho/\mu})_{\mathrm{wall}}$. In this expression z^+ is the distance from the wall expressed in "wall coordinates," where the wall shear stress τ is used for normalization, and A^+ is an effective sublayer thickness in the same coordinates. A^+ is a function of the pressure gradient, wall roughness, and blowing. In the

outer wake region of the boundary layer the mixing length is modeled as being a constant proportional to the boundary layer thickness; thus if $z > \lambda\delta_{99}/\kappa$

$$\ell = \lambda\delta_{99} \tag{8}$$

Thus, for the modeling of the mixing length three constants are involved, i.e., κ, λ, and A^+. Details of this model are given in Ref. 11.

The current distribution and electric fields were found for an assigned average current in the y direction by solution of Maxwell's equations with the assumption of infinite segmentation so that the average current in the x direction was zero. The variable properties and velocity as a function of z were obtained from the last step of the boundary layer solver and the calculated current densities and electric fields were then used in the boundary-layer code.

Numerical Techniques

The boundary-layer equations just given were solved using a finite difference scheme based on a boundary-layer code developed at Stanford and known as STAN5.[14] It was necessary to modify STAN5 to include the J_yB term in the momentum equation and the $\boldsymbol{J}\cdot\boldsymbol{E}$ term in the energy equation. A second modification to STAN5 was made to provide a stable scheme for the computation of internal flows. This involved using a separate core solver to calculate the pressure gradient and the outer boundary-layer conditions. Details are given in Ref. 11.

III. Experimental Technique

The laser anemometer system used in this work has been reported in detail elsewhere[11,15] and only its essential features will be discussed here.

A dual beam, real-fringe system was used in (near) forward scatter with access obtained via mirrors through open ports in the top and bottom electrode walls as shown in Fig. 2. The measurement volume was ~0.25 mm in diameter and ~4 mm long (y direction) and could be scanned in the z direction by translating the transmitting and receiving optics together. The fringe spacing was 15.2 μm, yielding a Doppler frequency of ~16 MHz for U~240 m/s. Particles of ZrO_2 (~1 μm size) were supplied by injecting a paste of powder, glycerin, and ethanol into the fuel line by a mechanically driven piston, at a rate of ~1 g/min to obtain a data rate of ~5000/s.

The detected signals were processed by a counter-type processor (TSI 1096) having an effective clock frequency of 500 MHz, which yields a velocity resolution of ~0.2%. The digital data output from the counter were fed to a minicomputer which processed sets of 8 data blocks each of 2048 signals at each measurement station. The computer processed the ~16 K individual velocity measurements to output, on-line, the mean velocity, the turbulence intensity, and a histogram of the velocity probability density.

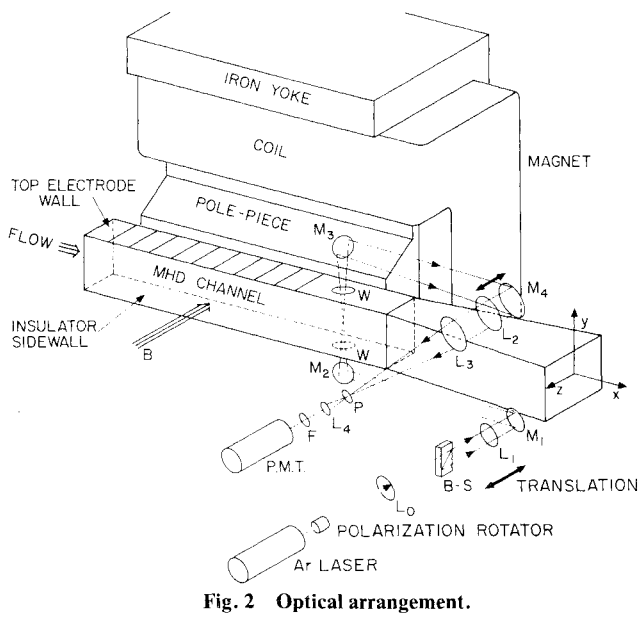

Fig. 2 Optical arrangement.

Table 1 Channel configuration

Construction: MgO lined water-cooled metal shell
Channel dimensions
Height: 0.10 m (between electrode walls)
Width: 0.05 m (between insulating walls)
Channel inlet to:
First electrode: 0.60 m
Last electrode: 1.06 m
Measurement point: 1.10 m
Electrodes
Number: 13
Size: 5.00 × 1.85 cm
Pitch: 3.8 cm
Material: Type 310 stainless steel
Cooling: Water cooled copper back plate
Operating temperature: 1000-1350 K
Magnetic field: 2.4 T, uniform over electrode area

IV. Experimental Results and Comparison with Computations

The generator configuration used in the experiments is shown schematically in Fig. 3. The dimensions of the channel are given in Table 1. The measurement point, at the center of the insulating wall, was located 24 channel widths downstream from the nozzle. The channel, 10 cm high by 5 cm wide, was operated at a total mass flowrate of 0.11 Kg/s with a nitrogen to oxygen (N_2/O_2) ratio of 0.5 by weight. Adjacent electrodes were paired and augmented with 240 V to produce an average current density of 0.74 amp/cm^2 based on total current and electrode wall area. This current density resulted in a Hartmann number based on current density of 26. The Reynolds number was 8200, based on the channel half width. Table 2 summarizes the flow conditions.

Velocity profiles were measured for three different generator conditions. The first profile was a control case measured with zero magnetic field and current. This profile was used as a basis of comparison for the other two profiles and for the adjustment of parameters in the numerical calculations to account for hydrodynamic effects in the channel not included in the present model. The second profile was measured with a magnetic field of 2.4 T, but with the generator open circuited, so that there was no net current. The third profile was measured with a magnetic field of 2.4 T and with the generator operated in an augmented short-circuit mode. The second and third profiles were obtained at nearly

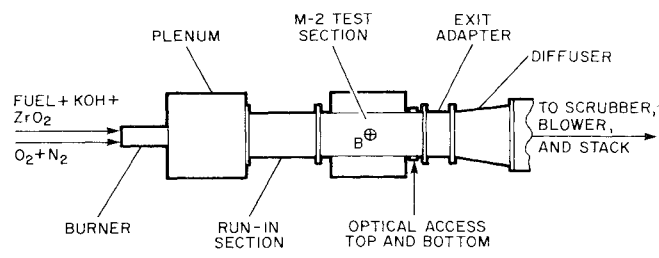

Fig. 3 Generator configuration for measurement of insulating wall boundary layer.

Table 2 Flow conditions

Fuel: Ethanol
Oxidizer: Stoichiometric amount of oxygen
Diluent: Nitrogen, N_2/O_2 0.5 by weight
Seed material: KOH dissolved in fuel
Amount of seed: 1% potassium in flow by weight
Anemometry particles: Zirconia 0.5-2 μm diam
Flux of particles: 0.65 g/min
Total flowrate: 0.11 Kg/s
Plenum heat loss: 130 Kw
Flame temperature: 2760 K
Electrode temperature: 1075-1200 K
Insulating wall temperature: 2000 K
Mean core velocity: 200 m/s
Fluid properties at channel inlet;
Density: 0.13 Kg/m^3
Viscosity: 8.2×10^{-5} Kg/m-s
Thermal conductivity: 0.19 J/m-s-K
Electrical conductivity: 11.5 mho/m
Nondimensional parameters based on channel half width
Reynolds number: 8200
Classical Hartmann number: 23
Current Hartmann number: 26
Length Reynolds number: 3.6×10^5

the same time by making velocity measurements with and without current at each point in the boundary layer.

The velocity profile and the turbulence intensity (normalized on the core average velocity) measured for the control case are shown in Figs. 4 and 5. Figure 4 shows a calculated profile as a solid line. One of the primary purposes of the control profile was to provide a case against which the calculations could be compared without MHD effects. The control profile was fuller than would be expected from a standard boundary layer. Daily,[1] in measurements of the electrode wall boundary layer, also found the velocity profile to be fuller than was predicted by calculations. In the present profiles, however, this effect is even more pronounced than in those measured by Daily.

With cold air flowing over smooth plates, investigators have used values of $\kappa=0.41$, $\lambda=0.084$, and $A^+=26$ to obtain good agreement between theory and experiment. The insulator wall channel construction for the present experiments used MgO ceramic pieces about 2 in. long in the flow direction and loosely fitted to permit thermal expansion during high temperature operation. Temperature gradients in the ceramic pieces caused bowing toward the channel center so the wall surface condition was not well defined. Inspection after cooldown suggested that steps at 2-in. intervals as much as 2 mm high could be expected. Because of this unavoidable uncertainty in the condition of the wall, it was decided to select boundary-layer parameters that gave a good fit to the data for the $J=B=0$ case and not change them for the other cases. In this way the uncertain wall conditions could be accounted for and the effects of magnetic field and current could be observed. Work is continuing at Stanford to improve the understanding of the turbulence parameters so that a less ad hoc selection can be made. For the solid curves in Fig. 4, the following parameters were used: $\kappa=0.6$, $\lambda=0.6$, and $A^+=43$. Good agreement with the experimental data was obtained.

The calculated and measured velocity profiles for a magnetic field of 2.4 T and with the generator in open-circuit operation are also shown in Fig. 4. The associated measured turbulence intensity profile is given in Fig. 5. The open-circuit profile would be expected to be fuller than the control case due to the effect of recirculating currents in the channel. However, the profiles with and without magnetic field actually show no significant difference. There are two reasons for this. The first is that the control profile is already sufficiently full so that the small effect does not show up. The second reason is that turbulence damping (Sonju[5]) acts to reduce the fullness of the profile, thus working against the Hartmann effect. A single solid curve is shown for the control case ($B=J=0$) and the $B=2.4$, $J=0$ case.

At each measurement position, augmented short-circuit data were obtained alternately with the open-circuit data. The velocity profile for the augmented short-circuit case is again presented in Fig. 4, and the turbulence intensity is shown in Fig. 5. The velocity profile clearly shows that the maximum velocity occurs not at the center of the channel, but near the wall. This phenomenon is unique to extended Hartmann flow and does not occur in classical Hartmann flow. The effect is a result of the rapid decrease of the current density toward the wall, and hence of the MHD body force, due to the decrease in electrical conductivity near the cool wall. This reduction of MHD body force causes an increase of velocity near the wall relative to the $B=0$ case. The alteration in velocity profile increases the skin friction and, through convection effects, also increases the heat transfer. Although the velocity overshoot phenomenon is clear evidence of extended Hartmann flow, a simple steepening of the boundary layer can

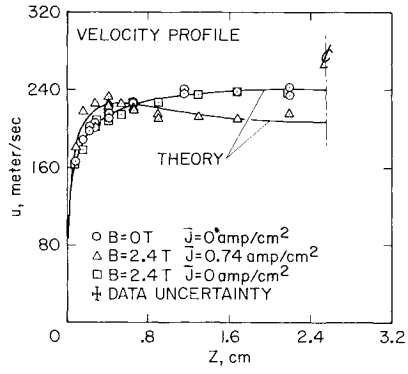

Fig. 4 Sidewall velocity profiles.

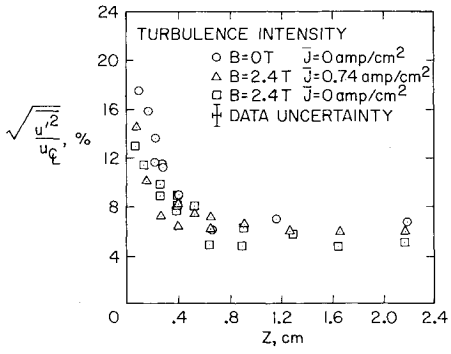

Fig. 5 Sidewall turbulence intensity profiles.

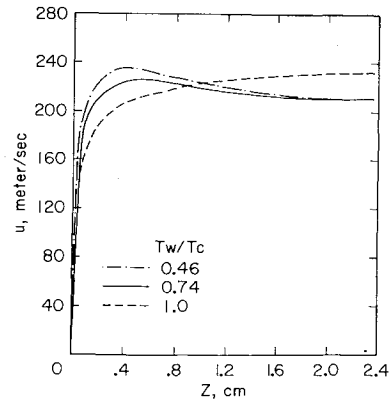

Fig. 6 Effect of wall temperature on extended Hartmann flow velocity profiles.

Table 3 Pilot plant generator conditions

$B = 6\ T$		$U = 800$ m/s		Height = 0.5 m			T(electrode) = 2000 K	
x, m	P, atm	T, K	A, m^2	E_x, kV/m	V_{out}, V	V_{loss}, V	J_y, A/cm^2	P_{out}, MW
0.20	5.00	2835	0.079	-----	-----	---	-----	0.0
0.46	4.73	2821	0.084	0.93	1673	121	1.67	1.2
0.98	4.47	2807	0.089	0.96	1670	131	1.54	2.4
2.02	3.28	2735	0.119	1.20	1655	176	1.19	8.4
3.06	2.50	2673	0.154	1.41	1644	220	0.96	13.4
4.10	1.87	2608	0.201	1.62	1632	277	0.74	18.4
5.14	1.39	2542	0.264	1.75	1620	351	0.53	23.3
5.92	1.13	2494	0.320	1.76	1610	409	0.39	26.7
6.96	0.87	2436	0.404	1.69	1597	478	0.25	30.4
7.48	0.78	2409	0.448	1.63	1590	505	0.20	32.0

occur without the overshoot under some conditions. The Hartmann number of 26 in the present experiments is about the value to be expected in a commercial MHD power plant in which both the velocity and magnetic field would be higher than for the present measurements.

In order to make the numerical calculations for comparison with the experimental data, it was necessary to have an estimate of the wall temperature. The wall temperature was not measured in the present tests but was based on numerous past measurements which showed values of about 2000 K. This figure, corresponding to a wall to core temperature ratio of 0.74, was used to fit the data. As can be seen in Fig. 4, the agreement between theory and experiment is very good. To indicate the effect the wall temperature has on the profile, Fig. 6 shows the calculated profiles with several different wall temperatures, but with the other conditions held constant. With a wall to core temperature ratio of unity, the calculated profile is not modified by extended Hartmann flow. As the wall to core temperature ratio is decreased an overshoot occurs. A further decrease in the temperature ratio increases the amount of overshoot.

V. Computations for Large Generators

Pilot Plant Generator

To determine the importance of extended Hartmann flow and turbulence damping on a larger-scale generator, calculations were performed for a 250 MW_{th} pilot plant generator burning coal in preheated air. A segmented Faraday generator operating subsonically at a constant velocity and a magnetic field strength of 6 T was modeled. An insulator wall temperature of 2000 K was assumed for the calculations.

A one-dimensional MHD computer program was run to determine the operating conditions for high enthalpy extraction. The generator conditions used by the boundary-layer program are summarized in Table 3. The power output of this channel is calculated to be 32 MW for a 13% enthalpy extraction and a 61% turbine efficiency, as opposed to 40.7 MW or 16% enthalpy extraction obtained in Ref. 16 in a similar calculation that excluded electrode voltage drops. The current density obtained in these calculations served as input for the boundary-layer code.

For each of the two generator cases to be presented, two calculations were made. The first calculation for the insulator wall boundary layer was computed according to the present model where the current density varies across the channel. The second calculation will be called the control calculation in which the current density is held constant across the channel such that the average current density is the same in both calculations. This form of control calculation was chosen in preference to letting either the current or the magnetic field go to zero because in the latter cases the conditions in the generator would be significantly different. The control calculation and the variable current calculation have the same average momentum loss due to the interaction of the current with the magnetic field. Thus the flow conditions along the channel are approximately the same for both the variable current and control calculations. In these calculations, a simple integral expression is used to compute the electrode wall displacement thickness which is then used in the core program to determine the effective area. The normally accepted values of the turbulence parameters were used for the pilot plant generator calculations. Thus 0.41, 0.085, and 26 were assigned for κ, λ, and A^+, respectively.

The skin friction coefficient computed for the pilot plant generator case is presented in Fig. 7. The effect of extended Hartmann flow is seen to significantly increase the skin friction by up to about 160% over that for the control case.

The Stanton number for the pilot plant generator is shown in Fig. 7. The increase in heat transfer is about 53% over the uniform current case, which is more modest than the increase in the skin friction. This increase in heat transfer is due primarily to the steepening of the velocity profile that results in increased convection of energy toward the wall and thus steepening of the temperature gradient at the wall. Joule heating effects are minimal in the insulating wall boundary layer since the current is shunted around the low conductivity region near the wall.

Supersonic Generator

The second generator examined was a supersonic generator. This case is presented because it yields important insight into the mechanism by which extended Hartmann flow affects the boundary layer. The generator considered is a constant

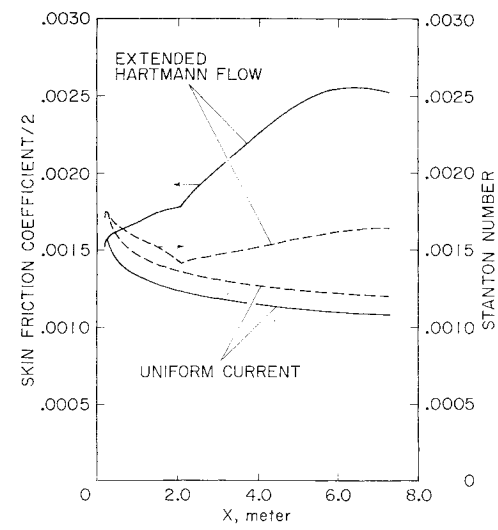

Fig. 7 Pilot plant generator skin friction and Stanton number comparisons.

velocity high Mach number generator operating at a velocity of 2500 m/s or a Mach number of 2.7. The generator has a constant height of 0.5 m with an inlet width of 0.5 m. After 2.25 m of active generator section in which the magnetic field is a constant 5 T, the channel exit is 3.7 m wide. The thermal power input to the generator is 1000 MW with 130 MW electrical output. The stagnation temperature is 3100 K and the static temperature at the channel inlet is 2360 K. The insulating wall temperature is 2000 K. The current density in the generator varies linearly from 1.25 amp/cm^2 at $x=0.25$ m to 1.53 amp/cm^2 at $x=2.25$ m. The inlet channel pressure is 2.0×10^5 N/m^2, while the channel exit pressure is assumed to be 2.0×10^4 N/m^2, based on pressure recovery through a normal shock to atmospheric pressure. The standard turbulence constants were used so that κ, λ, and A^+ were 0.41, 0.085, and 26, respectively.

The calculated skin friction coefficient and Stanton number are presented in Fig. 8. In contrast to the pilot plant generator case, extended Hartmann flow causes lower skin friction and heat transfer, with the skin friction and heat transfer eventually approaching zero, indicating incipient flow separation. The reason for this behavior is connected with the temperature "overshoot" characteristic of supersonic boundary layers and the strong dependence of electrical conductivity on temperature. Figure 9 shows the electrical conductivity and the current density in the insulating wall boundary layer for extended Hartmann flow. The high electrical conductivity in the boundary layer gives rise to a high current density which leads to a large $\boldsymbol{J}\times\boldsymbol{B}$ braking force. Inasmuch as the static pressure gradient is determined largely by the core $\boldsymbol{J}\times\boldsymbol{B}$ force, the effective pressure gradient is more adverse in the insulating wall boundary layer than in the core. This effective adverse pressure gradient, in addition to reducing the steepness of the velocity profile near the wall, causes the insulating wall boundary layer to separate for a milder pressure gradient than the electrode wall boundary layer for high supersonic flow. This is contrasted with a subsonic generator, where extended Hartmann flow produces an effective positive pressure gradient, stabilizing the insulating wall boundary layer against separation, and steepening the velocity profile at the wall. However for supersonic MHD generators, it is believed that this effect has been overlooked, and separation on the sidewall may be an important practical problem in supersonic MHD generators.

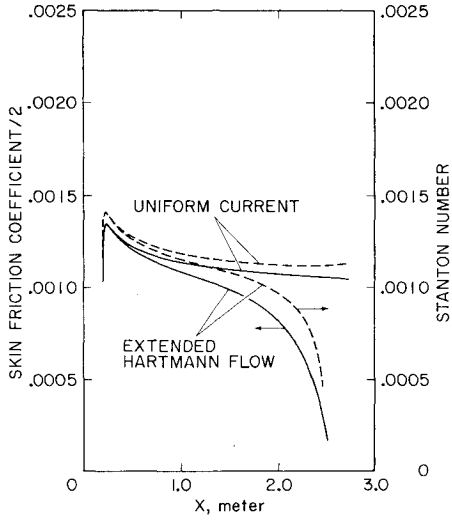

Fig. 8 Supersonic generator skin friction and Stanton number predictions.

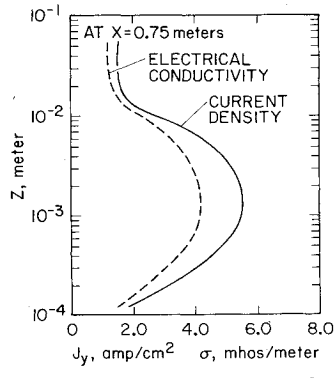

Fig. 9 Current density and electrical conductivity for supersonic generator.

The important conclusions about the generator calculations can be summarized as follows. In the pilot plant generator, extended Hartmann flow causes a significant increase in the skin friction on the insulating wall. The insulating wall boundary layer in the pilot plant generator will be more resistant to separation than the electrode wall boundary layer, due to the effective favorable pressure gradient generated in extended Hartmann flow. These conclusions can be contrasted with those made about the supersonic generator. Due to the temperature overshoot, the skin friction and heat transfer can exhibit decreases due to extended Hartmann flow that are relatively mild unless separation occurs in the boundary layer. This separation is more likely to occur on the insulating wall than the electrode wall. The effect of extended Hartmann flow is enhanced in the subsonic case by a lower wall temperature, but is is enhanced in the supersonic case by an increase in wall temperature that increases the temperature overshoot.

VI. Conclusions

Based on both theoretical calculations and experimental results, it has been shown that extended Hartmann effects on the insulator wall can be important in MHD generators. The steepening of the velocity profile due to a nonuniform current across the channel in the magnetic field direction was measured by laser anemometry and calculated by solution of the boundary-layer differential equations. For the conditions of the experiment, the maximum velocity was observed near the wall rather than in the channel core. Damping of the velocity fluctuations by the magnetic field was also observed in the experiments. This effect acts to decrease the skin friction and the heat transfer.

Computations appropriate for a pilot-plant size MHD generator were made and the predictions indicated that the extended Hartmann effect increased the skin friction by 160% and the heat transfer by 53%. As a second case, a supersonic generator was considered. Extended Hartmann flow caused a reduction in both the skin friction and the heat transfer, and eventually led to separation of the boundary layer. This effect is attributed to the overshoot in temperature that can occur in supersonic boundary layers. For the subsonic case, extended Hartmann flow has a stabilizing effect against separation.

In conclusion, the present work has shown the importance of the inclusion of extended Hartmann flow in modeling the insulating wall boundary layer. This effect has been shown to markedly alter the shape of the insulating wall velocity profile, resulting in changes in the skin friction and the heat transfer rate. For the accurate design of future MHD generators, it is strongly recommended that this effect be included in the models used in the design process.

Acknowledgments

The generous assistance of many students and staff members of the High Temperature Gasdynamics Laboratory is gratefully acknowledged. Frank Levy, Philip Krug, and Kent James were especially helpful with testing, electronics, and computational concerns. This work was supported by the U.S. Department of Energy under Contract EX-76-C-01-2341.

References

[1] Daily, J.W., Kruger, C.H., Self, S.A., and Eustis, R.H., "Boundary-Layer Profile Measurements in a Combustion Driven MHD Generator," *AIAA Journal*, Vol. 14, Aug. 1976, pp. 997-1005.

[2] James, R.K. and Kruger, C.H., "Plasma Measurements of Joule Heating Effects in the Near Electrode Region of an Open Cycle MHD Generator," *Proceedings of the 18th Symposium on Engineering Aspects of Magnetohydrodynamics*, Butte, Mont., June 1979, pp. E.4.1-6.

[3] Hartmann, J. and Lazarus, F., "Kgl. Danske Videnskag Selskab," *Mathematisk-Fysiski Meddelelser Kongelige Danske Videnskabernes Selskab*, Vol. 15, No. 6, 1937, p. 7.

[4] Murgatroyd, W., "Experiments on Magneto-Hydrodynamic Channel Flow," *Philosophical Magazine*, Vol. 44, 1953, p. 1348.

[5] Sonju, O.K., "Viscous Magnetohydrodynamic Flows," Stanford University, SU-IPR Rept. 245, July 1968.

[6] Louis, J.F., Lothrop, J., and Brogan, T.R., "Fluid Dynamic Studies with a Magnetohydrodynamic Generator," *The Physics of Fluids*, Vol. 7, March 1964, p. 362.

[7] Teno, J., Liu, C., and Brogan, T.R., "Boundary Layers in MHD Generators," *Proceedings of the 10th Symposium on Engineering Aspects of Magnetohydrodynamics*, Cambridge, Mass., March 1969, pp. 15-22.

[8] Sonju, O.K., Teno, J., and Brogan, T.R., "Comparison of Experimental and Analytical Results for a 20 MW Combustion-Driven Hall Configuration MHD Generator," *Proceedings of the 11th Symposium on Engineering Aspects of Magnetohydrodynamics*, Pasadena, Calif., March 1970., pp. 5-10.

[9] Sutton, G.W. and Sherman, A., *Engineering Magnetohydrodynamics*, McGraw-Hill, New York, 1965.

[10] Mitchner, M. and Kruger, C.H., Jr., *Partially Ionized Gases*, Wiley & Sons, New York, 1973.

[11] Rankin, R.R., "Insulating Wall Boundary Layer in a Faraday MHD Generator," Stanford University, HTGL Rept. 106, April 1978.

[12] Pepper, J.W., "Effect of Nitric Oxide Control on MHD-Steam Power Plant Economics and Performance," Stanford Univ., SU-IPR Rept. 614, Dec. 1974.

[13] Kays, W.M., *Convective Heat and Mass Transfer*, McGraw-Hill, New York, 1966.

[14] Crawford, M.E. and Kays, W.M., "STAN5-A Program for Numerical Computation of Two-Dimensional Internal/External Boundary Layer Flows," NASA CR-2742, Dec. 1976.

[15] Self, S.A., "Boundary Layer Measurements in Combustion MHD Channels," 3rd International Workshop on Laser Velocimetry, Purdue Univ., July 1978.

[16] Burton, T., et al., "CDIF-MHD Generator System Conceptual Design," ERDA Rept. TID-27150, Dec. 1976.

From the AIAA Progress in Astronautics and Aeronautics Series

SPACE SYSTEMS AND THEIR INTERACTIONS WITH EARTH'S SPACE ENVIRONMENT—v. 71

Edited by Henry B. Garrett and Charles P. Pike, Air Force Geophysics Laboratory

This volume presents a wide-ranging scientific examination of the many aspects of the interaction between space systems and the space environment, a subject of growing importance in view of the ever more complicated missions to be performed in space and in view of the ever growing intricacy of spacecraft systems. Among the many fascinating topics are such matters as: the changes in the upper atmosphere, in the ionosphere, in the plasmasphere, and in the magnetosphere, due to vapor or gas releases from large space vehicles; electrical charging of the spacecraft by action of solar radiation and by interaction with the ionosphere, and the subsequent effects of such accumulation; the effects of microwave beams on the ionosphere, including not only radiative heating but also electric breakdown of the surrounding gas; the creation of ionosphere "holes" and wakes by rapidly moving spacecraft; the occurrence of arcs and the effects of such arcing in orbital spacecraft; the effects on space systems of the radiation environment, etc. Included are discussions of the details of the space environment itself, e.g., the characteristics of the upper atmosphere and of the outer atmosphere at great distances from the Earth; and the diverse physical radiations prevalent in outer space, especially in Earth's magnetosphere. A subject as diverse as this necessarily is an interdisciplinary one. It is therefore expected that this volume, based mainly on invited papers, will prove of value.

737 pp., 6 × 9, illus., $30.00 Mem., $55.00 List

TO ORDER WRITE: Publications Dept., AIAA, 1290 Avenue of the Americas, New York, N.Y. 10104